22nd International Conference on Sustainable Energy Technologies
Kuala Lumpur, Malaysia, 13 to 15 August 2026 · ISBN 978-1-995850-00-9 · ISSN 2978-4387

CONFERENCE PAPER · LOW-CARBON BUILDINGS

A Photothermally Driven Moisture-Pumping Aerogel for Continuous and Directional Building Humidity Regulation

Yingying Yang[1*], Shuaijun Li[1], Ryad Bouzouidja[2], Tingting Vogt-Wu[2], Judith Lukau M'Nyampara[2], Marie Duquesne[3], Patrick Salagnac[3]

[1] School of Energy and Power Engineering, University of Shanghai for Science and Technology, Shanghai, China
[2] Univ. Bordeaux, CNRS, Bordeaux INP, I2M, UMR 5295, F-33400, Talence, France
[3] La Rochelle Université, LaSIE UMR CNRS 7356, Avenue Michel Crépeau, La Rochelle Cedex 1, 17042, France

RECEIVED 6 May 2026 · REVISED 9 June 2026 · ACCEPTED 21 June 2026
PRESENTED 13 to 15 August 2026 · PUBLISHED 23 November 2026

ABSTRACT

The development of passive humidity-regulating materials is essential for enabling zero-energy dehumidification in buildings. Herein, we report a trilayer cellulose-aerogel moisture pump capable of continuous and directional dehumidification, thereby addressing the limitations of conventional intermittent adsorption–regeneration cycles. Its asymmetric architecture, composed of hydrophilic and hydrophobic layers, promotes directional vapor transport, while lithium chloride incorporation provides a high hygroscopic capacity of 2.19 $g \cdot g^{-1}$ at 97% RH within 8 h. A multi-walled carbon nanotube photothermal layer enables rapid regeneration, reaching 53.7 °C within 15 min under one-sun irradiation and achieving complete desorption within 4 h. In a confined chamber with continuously humidifying, the proposed material maintained stable indoor humidity at 50 ± 2% RH for over 10 h, compared with a rapid rise to 80% RH within 1 h without the material. Furthermore, the moisture pump flexibly directs vapor transport from indoor spaces to environments of varying humidity levels, demonstrating robust directional performance. This study introduces a novel materials design strategy toward zero-energy, sustainable building humidity control.

KEYWORDS Building humidity regulation, Cellulose aerogels, Moisture pump, Building envelopes

1. Introduction

Air humidity plays a critical role in indoor environmental quality, thermal comfort, and industrial process reliability (Xie *et al.* 2025). In buildings, indoor relative humidity is closely associated with human health and comfort, with 40–60% RH generally considered a suitable range for indoor environments (Hu *et al.* 2023).

From an energy perspective, humidity control represents a major latent-load component of air-conditioning systems. Recent studies have shown that moisture management can account for a considerable fraction of building operational energy consumption (Woods *et al.* 2022; Pérez-Lombard *et al.* 2008). For building applications, the relevance of a humidity-regulating material depends not only on its equilibrium water uptake, but also on its moisture removal flux, regeneration energy source, durability under cyclic adsorption-desorption, integration mode within the envelope or ventilation path, and ability to operate under realistic indoor-outdoor vapor pressure gradients (Kreiger and Srubar 2019). Therefore, material-level performance must be linked to building-level indicators such as indoor RH stabilization, latent-load reduction potential, and operating stability under variable outdoor humidity (Qin *et al.* 2022).

* Corresponding author. Email address: yingyingyang@usst.edu.cn (Yingying Yang)

© 2026 The Author(s).
Published by Caravel Press.

doi.org/10.65582/set.2026.021

However, most currently studied composite dehumidification materials still operate in intermittent mode, where moisture absorption and regeneration processes alternate cyclically (Li and Yan 2025; Entezari *et al.* 2023). Once the hygroscopic material reaches saturation, the absorption process must be halted for thermal regeneration, thereby preventing continuous dehumidification. To address this limitation, researchers have proposed the concept of a moisture pump (Li *et al.* 2019; Cao *et al.* 2019; Zhang *et al.* 2000). Under thermal driving forces, such pumps can continuously extract moisture from indoor environments and transfer it outdoors, enabling solar-powered, continuous directional dehumidification (Entezari *et al.* 2023; Zhang *et al.* 2020; Yu *et al.* 2024). The key to achieving high-performance moisture pumps lies in the composite materials possessing three essential characteristics: ultrahigh moisture absorption capacity, rapid absorption-regeneration kinetics, and efficient moisture transport channels (Zhang *et al.* 2020). Although CA-based composites have made significant progress in both high moisture absorption capacity and solar-driven regeneration, compared to membrane-based moisture pumps, CA faces greater challenges in directional moisture transport due to its greater thickness. Therefore, how to simultaneously and synergistically optimize the three functions—moisture absorption, photothermal regeneration, and directional transport—within a thick, highly porous CA matrix remains a prominent challenge in materials design and engineering.

To address this challenge, this study proposes a photothermally driven Janus cellulose aerogel-based moisture pump for continuous and directional building humidity regulation (Cao *et al.* 2019; Zhang *et al.* 2000; Zhang *et al.* 2020; Yu *et al.* 2024). Inspired by natural unidirectional water transport phenomena observed in cedar trees (Wu *et al.* 2011) and pitcher plants (Dai *et al.* 2019), a hydrophilic/hydrophobic asymmetric wettability structure was constructed to promote moisture migration from the hygroscopic side toward the photothermal evaporation side. LiCl was introduced as the hygroscopic component to enhance moisture capture, while multi-walled carbon nanotubes (MWCNTs) were incorporated as the photothermal component to enable solar-driven regeneration. Through the integration of moisture absorption, directional moisture transport, and photothermal evaporation within a single aerogel framework, the resulting J-CNF/CNT@LiCl provides a self-regenerating moisture-pumping strategy for passive or hybrid humidity regulation in building envelopes, with potential to reduce the latent-load demand of conventional HVAC systems.

2. Materials, Fabrication, and Characterization Methods

2.1. Materials

The cellulose nanofibril aqueous suspension (CNF, solid content of 2 wt%) was provided by Songhu Shenjian Technology Co., Ltd. (China); anhydrous lithium chloride (LiCl, AR) granules were obtained from Xilong Scientific Co., Ltd. (China); multi-walled carbon nanotubes (MWCNT, purity >98%) were supplied by Shenzhen Suiheng Technology Co., Ltd. (China); methyltrimethoxysilane (MTMS) was purchased from Shanghai Macklin Biochemical Technology Co., Ltd.; and deionized water was prepared in the laboratory. All chemicals were used as received without further purification.

2.2. Solution preparation

Suspension A: A 5 g aliquot of 2 wt% CNF suspension was placed in a beaker, followed by the addition of 0.05 g of methyltrimethoxysilane (MTMS) for hydrophobic modification. The mixture was then stirred on a magnetic stirrer for 6 hours. Subsequently, 10 g of a 5 wt% LiCl solution was slowly added to the beaker, and solvent exchange was performed at 25 °C for 12 hours. After removing the excess surface solution, the resulting hydrophobic suspension was obtained and designated as Suspension A.

Suspension B: A 15 g aliquot of 2 wt% CNF suspension was placed in a beaker. Subsequently, 30 g of a 5 wt% LiCl solution was slowly added to the beaker, and solvent exchange was carried out at 25 °C

for 12 hours. After removing the excess surface solution, the resulting hydrophilic suspension was obtained and designated as Suspension B.

Suspension C: Into a beaker containing 10 mL of deionized water, 2.5 g of 2 wt% CNF and 0.1 g of MWCNTs were added. The mixture was then ultrasonicated to achieve homogeneity and designated as Suspension C.

2.3. Preparation of J-CNF/CNT@LiCl

As illustrated in Figure 1, suspension A was placed in a cylindrical mold (6 cm diameter). The mold was gently agitated to level the liquid surface and remove air bubbles, then transferred to a freezer for 1 hour to allow pre-freezing and shaping. Subsequently, Suspension B was poured onto the surface of the pre-frozen gel. After leveling the liquid surface, the mold was placed in the sample chamber of a freeze-dryer. The sample was frozen at −50 °C for 4 hours, followed by freeze-drying (−50 °C, 0.5 MPa) for 48 hours to obtain a bilayer aerogel with hydrophilic/hydrophobic properties (thickness ratio 3:1), designated as J-CNF@LiCl. A controlled amount of Suspension C was then uniformly coated onto the hydrophilic surface of the prepared J-CNF@LiCl. The sample was subsequently dried in the freeze-dryer for 12 hours and retrieved, designated as J-CNF/CNT@LiCl.

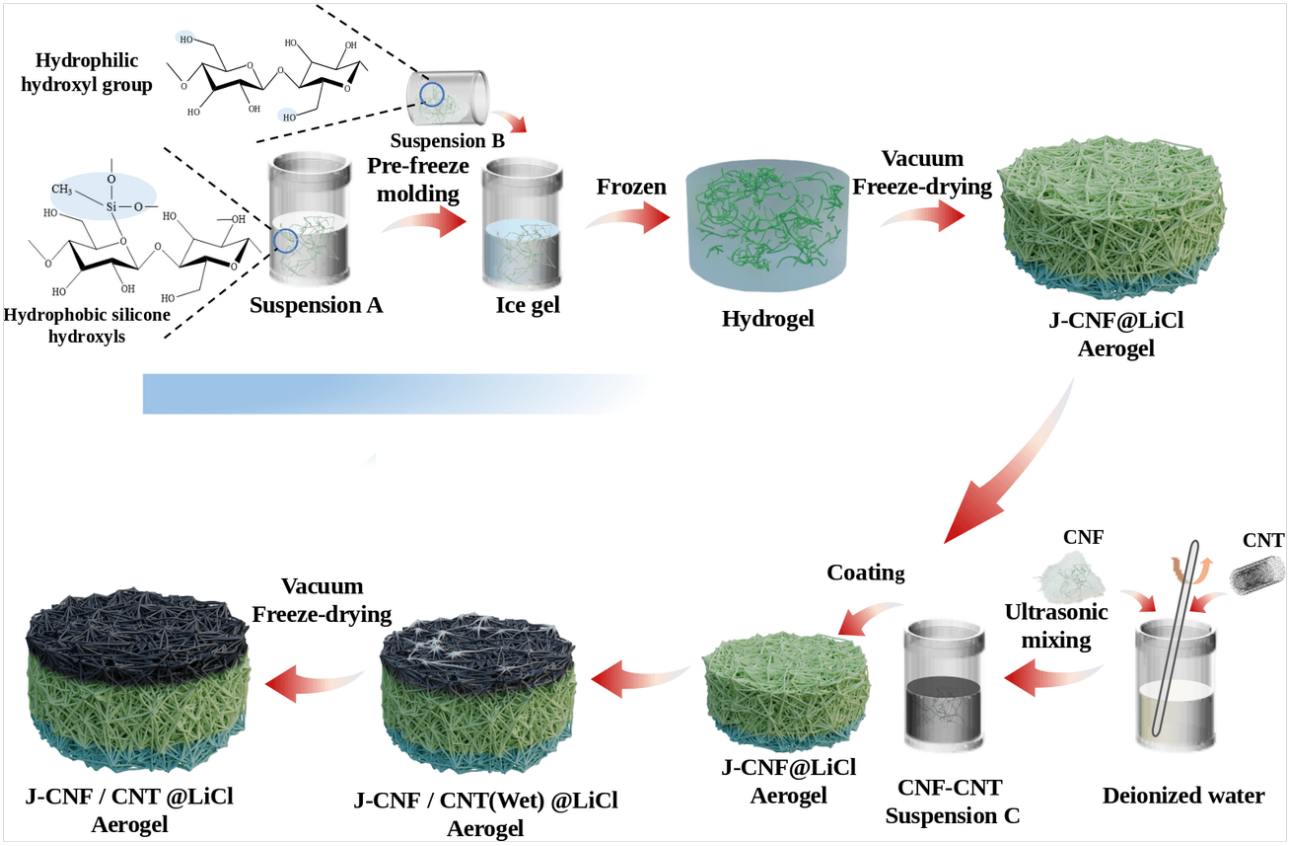

Figure 1. Preparation process of J-CNF/CNT@LiCl.

3. Results and discussion

3.1. Directional moisture transport performance

As illustrated in Figure 2a, when a water droplet deposits on the hydrophobic surface, it forms a distinct spherical cap morphology (average water contact angle $\theta \approx 127°$). This geometric confinement creates substantial hydrostatic pressure (HP) ($\Delta P \approx 2\gamma/R$, where R is the droplet curvature radius) at the gas-liquid interface. When HP exceeds the hydrophobic force (HF) induced by capillary pressure on the hydrophobic side, the droplet penetrates the hydrophobic layer and migrates toward the hydrophilic matrix. Simultaneously, the capillary force (CF) in the hydrophilic layer promotes rapid

water diffusion. Conversely, when contacting the hydrophilic surface, the droplet immediately spreads (γ<10°) into a thin film, causing the interface curvature radius to approach infinity. This reduces the hydrostatic pressure difference to negligible levels, allowing the hydrophobic layer to completely suppress reverse water penetration at the hydrophilic-hydrophobic interface.

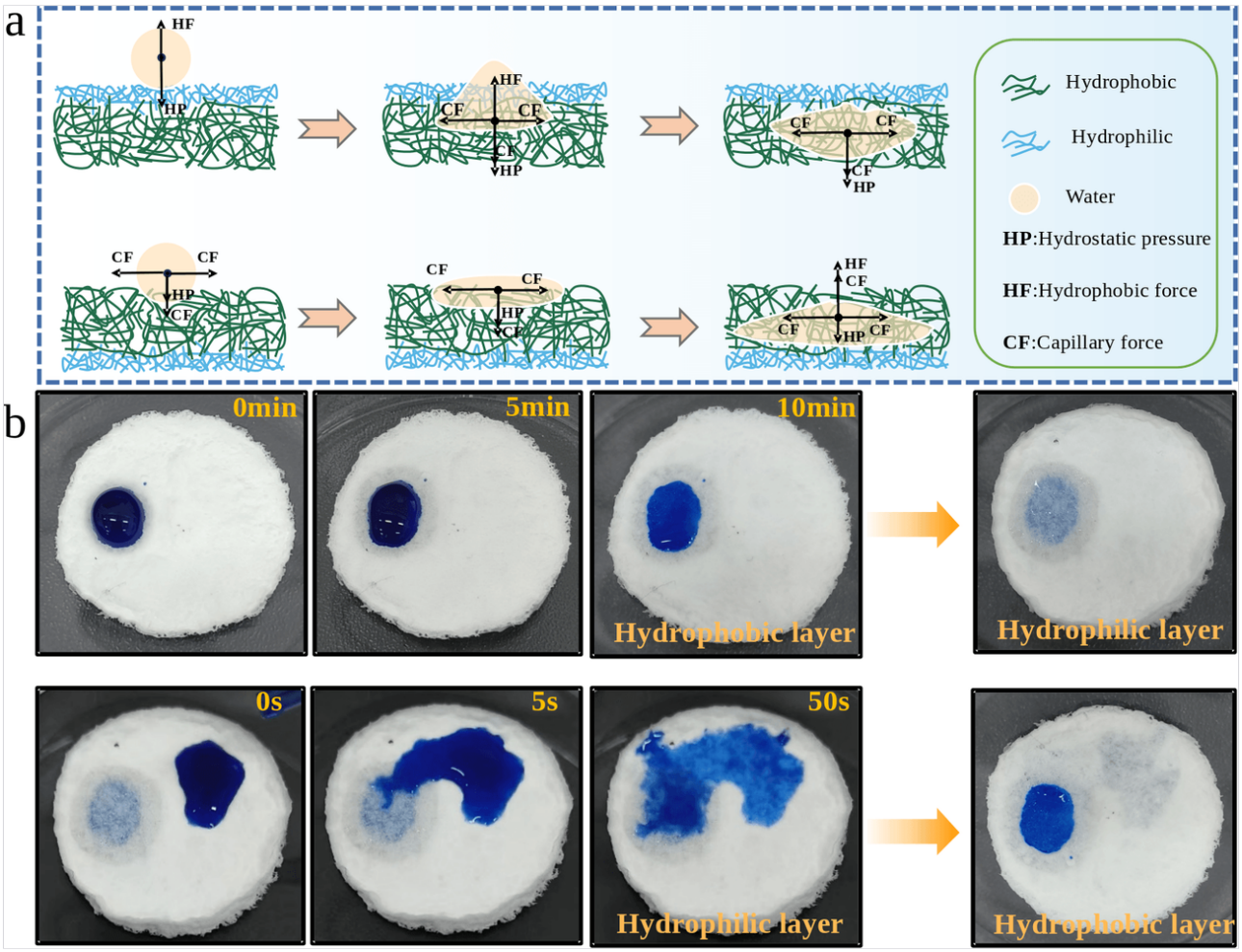

Figure 2. Directional water transport. (a) Schematic of directional transport driven by Janus wettability. (b) Penetration tests demonstrating directional water transport behavior in J-CNF@LiCl.

To experimentally validate this transport behavior, solution penetration and reverse penetration experiments were conducted (Figure 2b). When methylene blue solution was applied to the hydrophobic surface of J-CNF@LiCl, it permeated through to the hydrophilic layer, forming a distinct blue zone. However, when applied to the hydrophilic side, the solution only diffused radially within the hydrophilic layer, leaving merely a faint blue mark at the interface without penetrating the hydrophobic layer. This asymmetric penetration confirms that Janus wettable aerogels can effectively regulate water transport pathways through their unique hydrophilic-hydrophobic heterostructure, enabling selective directional transport from hydrophobic to hydrophilic layers. This asymmetric transport facilitates water delivery to the photothermal evaporation interface, which is a prerequisite for a non-membrane moisture pump.

To quantitatively evaluate the hygroscopic performance of the materials, systematic tests were conducted on CNF@LiCl, M-CNF@LiCl, and J-CNF@LiCl at 25 °C and 70% RH. Before testing, the samples were dried at 80 ± 2 °C until a constant weight was obtained. The dried samples were then placed in sealed desiccators containing saturated salt solutions, and the desiccators were kept in a constant-temperature chamber at 25 ± 0.5 °C to maintain a stable testing temperature. During the

adsorption process, the sample mass was recorded at predetermined time intervals. The moisture uptake capacity was calculated as (Equation 1):

$$q(t) = \frac{m(t) - m_0}{m_0} \quad (1)$$

Where:

- $q(t)$ = the water uptake capacity ($g \cdot g^{-1}$)
- m_0 = the dry mass of the sample (g)
- $m(t)$ = the sample mass after adsorption time t (g)

The results demonstrate comparable moisture uptake capacities among the three materials after 8 hours of absorption (Figure 3a), indicating that hydrophobic modification did not significantly affect the overall hygroscopic performance. This observation can be attributed to the fact that moisture uptake primarily originates from the hygroscopic and deliquescent behavior of LiCl distributed on the surface and within the CNF porous network, while hydrophobic modification only alters the surface wettability characteristics. To further verify this conclusion, comparative tests between J-CNF@LiCl and pure aerogel CA revealed that after 8 hours at 25 °C and 70% RH (Figure 3b), J-CNF@LiCl achieved a moisture uptake of 1.28 $g \cdot g^{-1}$, substantially higher than CA (0.059 $g \cdot g^{-1}$). This result conclusively demonstrates the dominant role of LiCl in the hygroscopic performance of the J-CNF@LiCl. Additional comparison with commercial Color Changing Silicone (0.11 g/g) further confirms the superior hygroscopic performance of the J-CNF@LiCl (Figure 3b). Considering the humidity variations across different climatic conditions, we systematically evaluated the hygroscopic performance of the J-CNF@LiCl at 25 °C under varying relative humidity levels (20%, 43%, 70%, and 97%) (Figure 3c). The experimental results show significantly enhanced moisture absorption capacity with increasing environmental relative humidity, primarily due to more extensive water molecule interactions with LiCl on both the surface and interior of J-CNF@LiCl under high-humidity conditions.

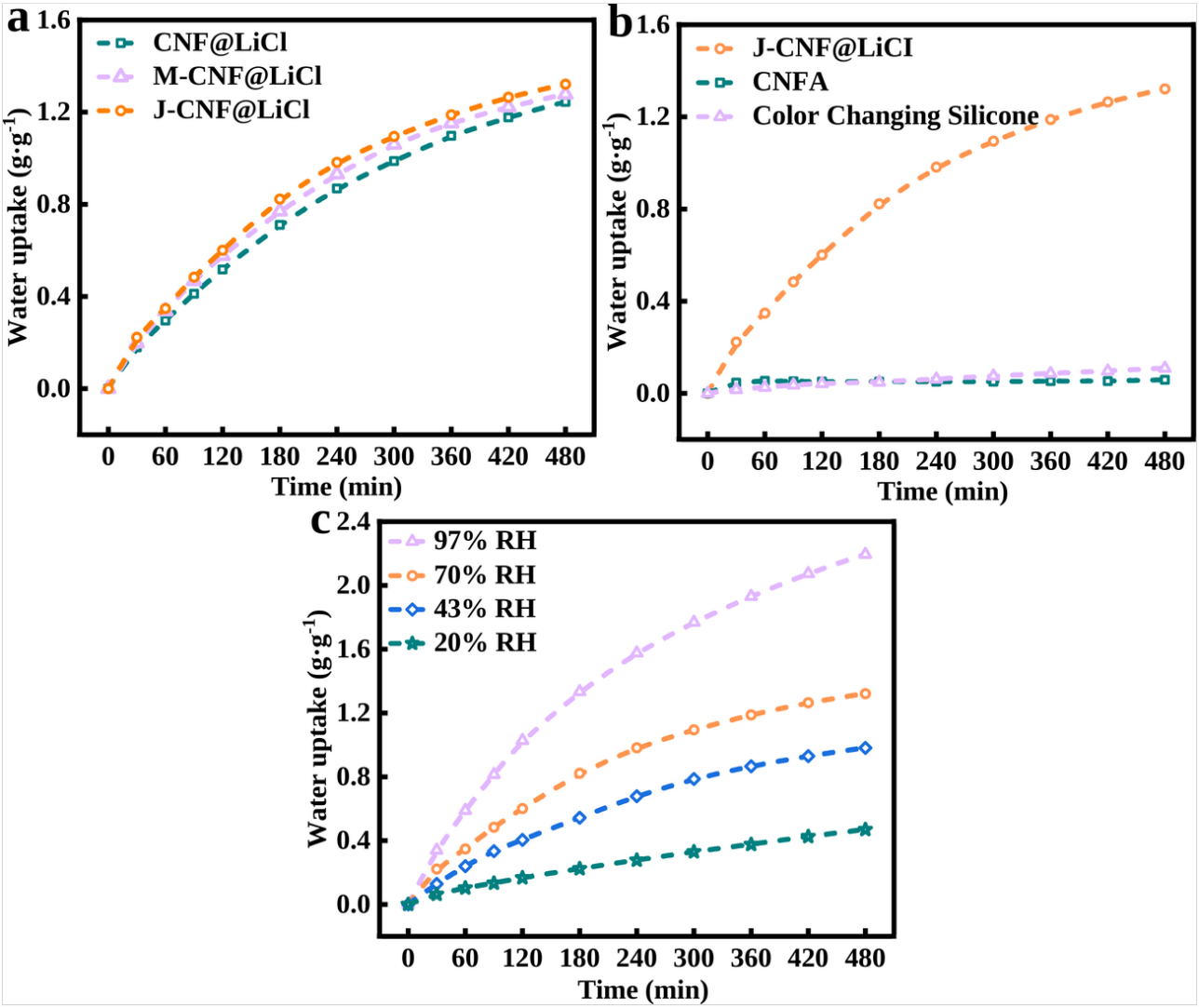

Figure 3. Comparative and humidity-dependent hygroscopic performance of J-CNF@LiCl. (a) Comparative hygroscopic performance at 70% RH and 25 °C among CNF@LiCl, M-CNF@LiCl and J-CNF@LiCl. (b) Comparative hygroscopic performance at 70% RH and 25 °C among J-CNF@LiCl, CA and Color Changing Silicone. (c) The hygroscopic performance of J-CNF@LiCl at 25 °C under various humidity conditions.

To further investigate the moisture absorption characteristics, the morphological evolution of CNF@LiCl and M-CNF@LiCl during a 24-hour absorption period at 25 °C and 70% RH (Figure 4) were recorded. Initial observations revealed both materials exhibited white, opaque solid characteristics. After 8 hours of moisture absorption, CNF@LiCl gradually transitioned from its edges toward the center into a semi-transparent state, while M-CNF@LiCl only showed localized semi-transparency at its peripheral regions. Following 24 hours of absorption, CNF@LiCl completely transformed into a semi-transparent state with distinct surface wetting characteristics. This behavior stems from its superior three-dimensional network structure that provides both hydrophilicity and water-retention capacity, effectively addressing potential leakage issues associated with deliquescent LiCl. In contrast, M-CNF@LiCl showed no significant surface wetting, but water droplets were observed at its edges, demonstrating the unique water-absorbing but non-retentive property of the hydrophobic layer. In the J-CNF@LiCl system, this design promotes directional water transport: moisture absorbed by the hydrophobic layer preferentially migrates outward and, under asymmetric wettability effects, transfers to the adjacent hydrophilic photothermal layer. This mechanism enables highly efficient water evaporation under photothermal driving forces. Such structural optimization not only

enhances moisture absorption performance but also creates favorable conditions for effective water evaporation.

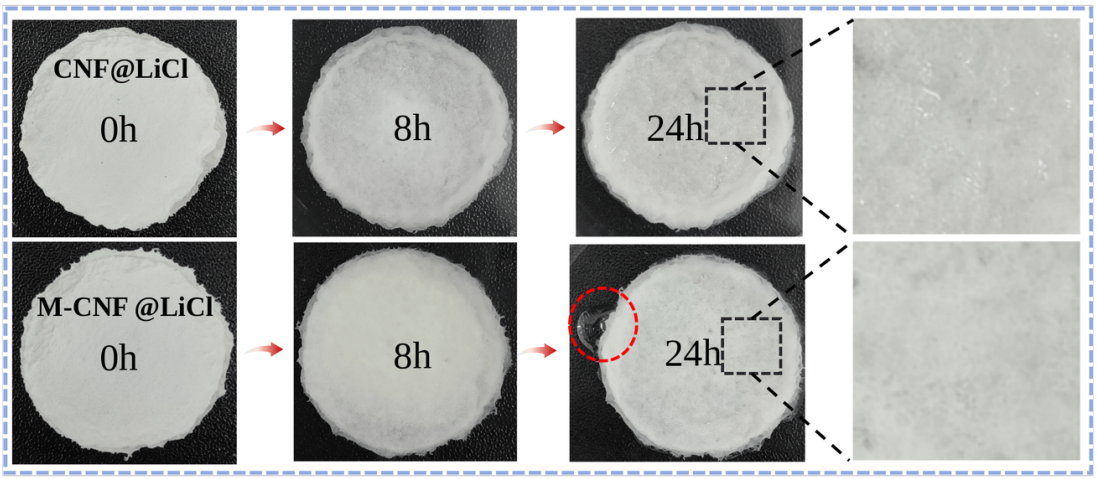

Figure 4. Morphological changes during moisture absorption at 70% RH and 25 °C for CNF@LiCl and M-CNF@LiCl.

3.2. Performance of the photothermal layer

To directly link photothermal conversion to the moisture desorption performance of J-CNF/CNT@LiCl, this study established a testing system. A xenon lamp was used as the solar simulator light source (spectral range 300–2500 nm). An electronic balance recorded the mass changes of J-CNF/CNT@LiCl in real time, while an infrared thermal camera monitored the temperature changes on the photothermal material surface. Using J-CNF@LiCl without a photothermal layer as control, both J-CNF@LiCl and J-CNF/CNT@LiCl were subjected to moisture absorption for 8 hours at 25 °C and 70% relative humidity before testing to ensure equal water weight absorption.

Figure 5b shows the surface temperature profiles of J-CNF/CNT@LiCl and J-CNF@LiCl under 1 kW m^{-2} illumination intensity. Both materials showed rapid temperature increase within the first 6 minutes of illumination, gradually stabilizing after 6 minutes, and reaching equilibrium after 15 minutes. Throughout this process, the average surface temperature of J-CNF/CNT@LiCl remained consistently higher than that of J-CNF@LiCl.

Notably, infrared thermal imaging (Figure 5a) revealed that J-CNF/CNT@LiCl reached a maximum average surface temperature of 53.7 °C, compared to only 38.3 °C for J-CNF@LiCl, demonstrating superior photothermal conversion performance that meets water evaporation requirements. Moreover, the uniform color distribution of temperature blocks across J-CNF/CNT@LiCl surface confirms the homogeneous distribution of MWCNTs on the hydrophilic layer, forming a photothermal layer with consistent light absorption capacity.

Further characterization using Ultraviolet-Visible-Near-Infrared (UV-Vis-NIR) spectroscopy (200–2500 nm) showed that J-CNF/CNT@LiCl exhibits full solar spectrum absorption characteristics with excellent light capture capability across the entire spectral range (Figure 5c), while J-CNF@LiCl demonstrated much weaker absorption. This conclusively proves that the outstanding photothermal conversion performance of J-CNF/CNT@LiCl originates from the constructed photothermal layer.

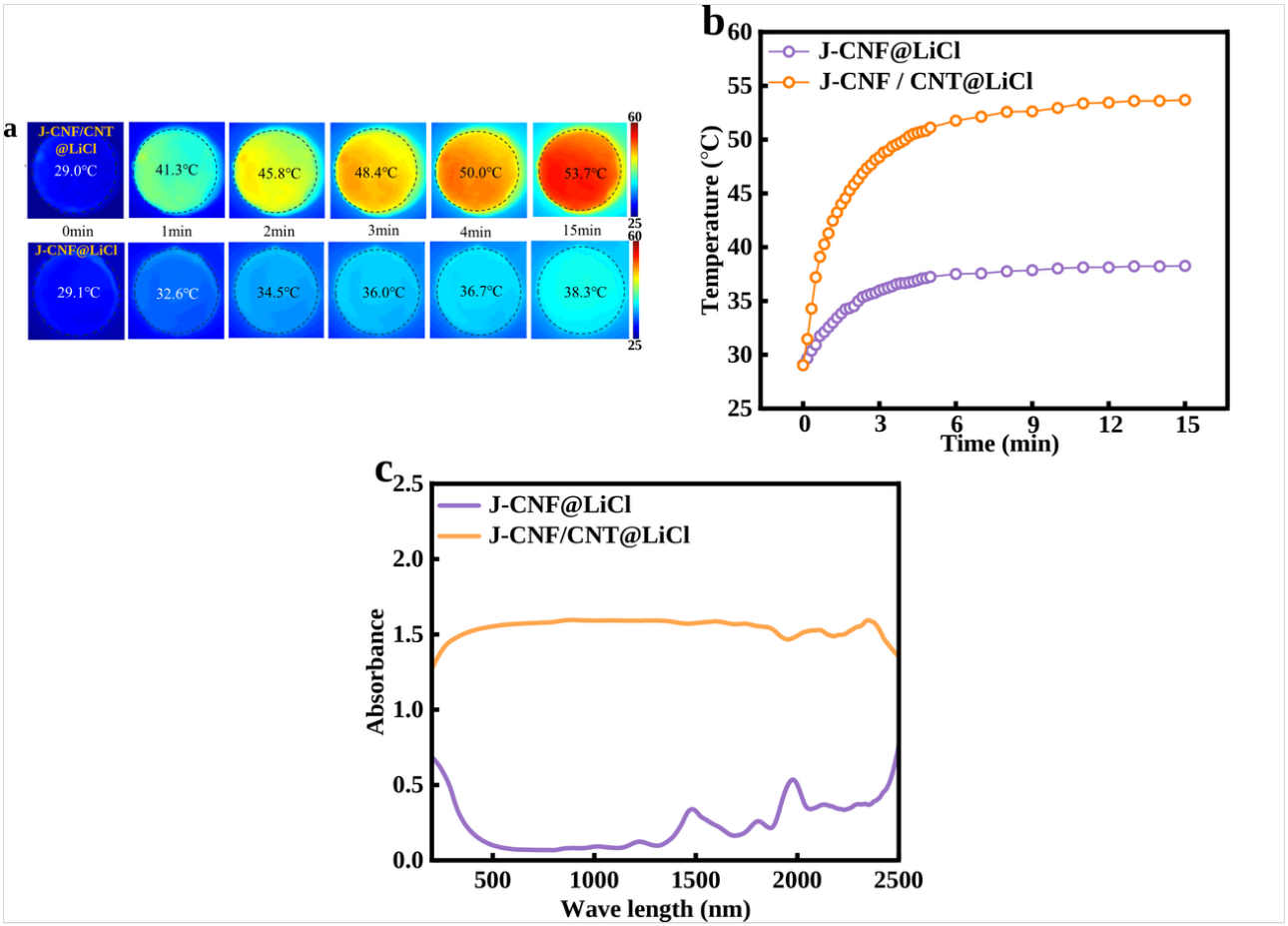

Figure 5. Photothermal response and broadband absorption characteristics of J-CNF/CNT@LiCl. (a) Infrared thermal images of J-CNF/CNT@LiCl and J-CNF@LiCl under 1 kW m^{-2} illumination intensity, recording surface temperature variations. (b) Surface temperature evolution curves of J-CNF/CNT@LiCl and J-CNF@LiCl under 1 kW m^{-2} solar irradiation. (c) Absorption spectra of J-CNF/CNT@LiCl and J-CNF@LiCl across the 200–2500 nm wavelength range.

3.3. Evaluation of continuous dehumidification performance of J-CNF/CNT@LiCl

To assess the device-level continuous directional dehumidification performance of J-CNF/CNT@LiCl as a moisture pump, a sealed simulated building system was constructed (Figure 6). The experimental setup included a 20×20×20 cm model house, a circular J-CNF/CNT@LiCl sample (6 cm diameter) serving as the dehumidification window. The entire system was placed within the large climate chamber.

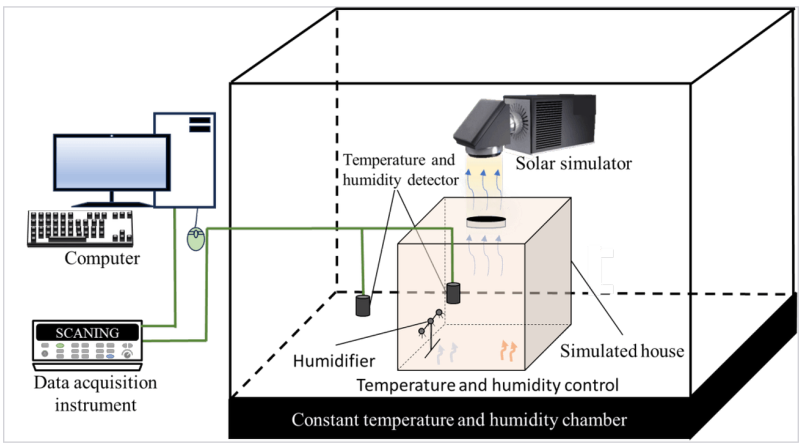

Figure 6. Schematic diagram of the simulated house testing system.

As shown in Figure 7, for the control group CNF@LiCl, the indoor humidity began deviating from equilibrium after 2 hours of testing and gradually increased. This occurred because the absorption capacity of the material progressively approached saturation during continuous operation, leading to declining absorption rates that ultimately failed to match the sustained moisture input. After 10 hours of continuous testing, the indoor relative humidity rose to 64.5%, exceeding the human comfort range (40–60% RH). In contrast, without any hygroscopic material, the indoor humidity reached 80% within just 1 hour, demonstrating the significant moisture capture capability of CNF@LiCl to maintain indoor humidity within the comfort range for extended periods.

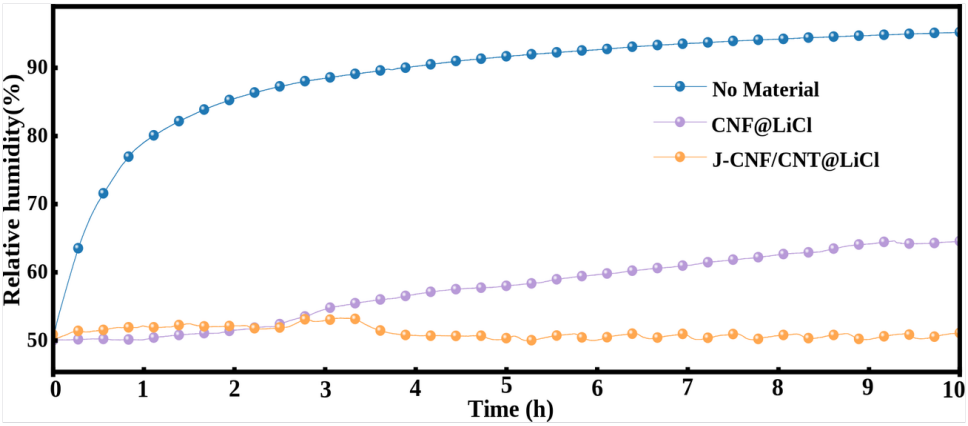

Figure 7. Dehumidification performance validation of J-CNF/CNT@LiCl and CNF@LiCl under sustained humidification.

The J-CNF/CNT@LiCl, equipped with a humidity pump function, demonstrates exceptional continuous dehumidification performance. Over a 10-hour testing period, the relative humidity inside the simulated house remained stable (50±2% RH). More importantly, post-test analysis revealed that the hygroscopic layer retained a well-dried state, confirming its sustained moisture uptake capability. This behavior arises from the synergistic interplay between the wettability characteristics of J-CNF/CNT@LiCl and transpiration effects: the absorbed water is continuously transported to the evaporation interface, where it is subsequently released via photothermal-driven evaporation, enabling regenerative cycling for continuous dehumidification. Such a unique humidity pump effect allows the material to overcome the saturation limitations of conventional hygroscopic materials, offering an innovative solution for indoor humidity regulation.

4. Conclusion

In this study, a trilayer cellulose aerogel-based moisture pump (J-CNF/CNT@LiCl) was fabricated using CNF as the substrate, which achieved continuous directional dehumidification. First, hydrophilic/hydrophobic layers were constructed to establish asymmetric wettability for directional moisture transport. Subsequently, the material demonstrated hygroscopic capacity and efficient light-to-heat conversion through the incorporation of the highly hygroscopic LiCl and a photothermal conversion layer of MWCNT. Static absorption tests (97% RH, 25 °C) revealed a moisture uptake capacity of 2.19 g/g after 8 hours. In photothermal conversion tests, the surface temperature of J-CNF/CNT@LiCl reached 53.7 °C within 15 minutes under 1-sun illumination, exceeding the control group (J-CNF@LiCl, 38.3 °C) by 15.4 °C. In dynamic continuous humidification experiments, J-CNF/CNT@LiCl maintained stable indoor humidity equilibrium at 50% RH (±2%) for over 10 hours, demonstrating excellent continuous dehumidification functionality. In contrast, without any hygroscopic material, the indoor relative humidity reached 80% within just 1 hour and kept increasing.

In summary, this study successfully developed a cellulose aerogel-based moisture pump. Its unique asymmetric wettability structure, efficient moisture absorption-desorption performance, and photothermal-driven regeneration capability provide a material-level pathway for the development

of passive, green humidity-regulating materials for continuous and directional dehumidification. Future work will focus on exploring long-term cyclic stability and scalability toward building-integrated prototypes under realistic environmental conditions.

Declarations

Author contributions. Yingying Yang: Conceptualization, Methodology, Investigation, Writing (original draft), Supervision, Writing (review and editing), Funding acquisition, Project administration. Shuaijun Li: Investigation, Formal analysis, Data curation, Writing (original draft). Ryad Bouzouidja: Methodology, Formal analysis, Writing (review and editing), Supervision, Funding acquisition, Project administration. Tingting Vogt-Wu: Formal analysis, Writing (review and editing), Supervision, Funding acquisition, Project administration. Judith Lukau M'Nyampara: Writing (review and editing), Supervision, Funding acquisition, Project administration. Marie Duquesne: Writing (review and editing), Supervision, Funding acquisition, Project administration. Patrick Salagnac: Writing (review and editing).

Funding. This work was supported·by the-National-Key R&D·Program of-China (No. 2026YFE0157900), the-Shanghai-Sci-tech-Co-research.Program (No. 26HB2706300) and the "PHC Cai Yuanpeprogramme (project number: 54527NF), funded-by the Frencch-MinistryMinistry of.for Europe·and Foreign Affairs, the· French Ministry forHigher Education, Research and Space, and the Chinese.Science and Technology (MOST)/the China ScholarshipCouncil (CSC). This workhas beenpartially funded-by the-CNFRS·Energyunit (Cellule Energie du CNRS) through the project FLASH (lowcarbon Functional MateriAls for-Sustainable thermal and·Humidity regulation).l

Conflicts of interest. not applicable

Data availability. Data

Acknowledgements. This work was supported by the National Key R&D Program of China (No. 2026YFE0157900), the Shanghai Sci-tech Co-research Program (No. 26HB2706300) and the “PHC Cai Yuanpei” programme (project number: 54527NF), funded by the French Ministry for Europe and Foreign Affairs, the French Ministry for Higher Education, Research and Space, and the Chinese Ministry of Science and Technology (MOST)/the China Scholarship Council (CSC). This work has been partially funded by the CNRS Energy unit (Cellule Energie du CNRS) through the project FLASH (lowcarbon FunctionaL MateriAls for Sustainable thermal and Humidity regulation).

References

Cao, Biye; Tu, Yaodong; Wang, Ruzhu (2019) 'A Moisture-Penetrating Humidity Pump Directly Powered by One-Sun Illumination', *iScience*, 15, pp. 502-513. Available at: https://doi.org/10.1016/j.isci.2019.05.013

Dai, Bing; Li, Kan; Shi, Lianxin; Wan, Xizi; Liu, Xi; Zhang, Feilong; Jiang, Lei; Wang, Shutao (2019) 'Bioinspired Janus Textile with Conical Micropores for Human Body Moisture and Thermal Management', *Advanced Materials*, 31(41). Available at: https://doi.org/10.1002/adma.201904113

Entezari, Akram; Lin, He; Esan, Oladapo Christopher; Luo, Weili; Wang, Ruzhu; You, Ruoyu; An, Liang (2023) 'Continuous humidity pump and atmospheric water harvesting inspired by a tree-pumping system', *Cell Reports Physical Science*, 4(2), pp. 101278. Available at: https://doi.org/10.1016/j.xcrp.2023.101278

Hu, Jiale; Wang, Yingying; Wang, Dengjia; Du, Hu; Fan, Jianhua; Liu, Yanfeng; Sun, Xin (2023) 'Indices for dynamic evaluation of indoor humidity and thermal environment', *Communications Engineering*, 2(1). Available at: https://doi.org/10.1038/s44172-023-00109-9

Kreiger, Brenton K.; Srubar, Wil V. (2019) 'Moisture buffering in buildings: A review of experimental and numerical methods', *Energy and Buildings*, 202, pp. 109394. Available at: https://doi.org/10.1016/j.enbuild.2019.109394

Li, Bangjun; Hua, Lingji; Tu, Yaodong; Wang, Ruzhu (2019) 'A Full-Solid-State Humidity Pump for Localized Humidity Control', *Joule*, 3(6), pp. 1427-1436. Available at: https://doi.org/10.1016/j.joule.2019.03.018

Li, Chun-Han; Yan, Wei-Mon (2025) 'Experimental and numerical study on heat and mass transfer of a membrane dehumidifier with various materials', *Journal of Building Engineering*, 106, pp. 112573. Available at: https://doi.org/10.1016/j.jobe.2025.112573

Pérez-Lombard, Luis; Ortiz, José; Pout, Christine (2008) 'A review on buildings energy consumption information', *Energy and Buildings*, 40(3), pp. 394-398. Available at: https://doi.org/10.1016/j.enbuild.2007.03.007

Qin, Menghao; Feaugas, Olivier; Zu, Kan (2022) 'Novel metal-organic framework (MOF) based phase change material composite and its impact on building energy consumption', *Energy and Buildings*, 273, pp. 112382. Available at: https://doi.org/10.1016/j.enbuild.2022.112382

Woods, Jason; James, Nelson; Kozubal, Eric; Bonnema, Eric; Brief, Kristin; Voeller, Liz; Rivest, Jessy (2022) 'Humidity's impact on greenhouse gas emissions from air conditioning', *Joule*, 6(4), pp. 726-741. Available at: https://doi.org/10.1016/j.joule.2022.02.013

Wu, Dong; Wang, Jian-Nan; Wu, Si-Zhu; Chen, Qi-Dai; Zhao, Shuai; Zhang, Hao; Sun, Hong-Bo; Jiang, Lei (2011) 'Three-Level Biomimetic Rice-Leaf Surfaces with Controllable Anisotropic Sliding', *Advanced Functional Materials*, 21(15), pp. 2927-2932. Available at: https://doi.org/10.1002/adfm.201002733

Xie, Mingxi; Chen, Erjian; Huang, Guorui; Jia, Teng; Dai, Yanjun (2025) 'Recent advancements in deep dehumidification technology: A review', *Renewable and Sustainable Energy Reviews*, 211, pp. 115321. Available at: https://doi.org/10.1016/j.rser.2024.115321

Yu, Jiaqi; Deng, Fangfang; Liu, Haoran; Wang, Chenxi; Zou, Hao; Wang, Ruzhu (2024) 'Passive and continuous moisture pump for humidity regulation via simultaneous water adsorption and desorption', *Device*, 2(6), pp. 100429. Available at: https://doi.org/10.1016/j.device.2024.100429

Zhang, L. Z.; Jiang, Y.; Zhang, Y. P. (2000) 'Membrane-based humidity pump: performance and limitations', *Journal of Membrane Science*, 171(2), pp. 207-216. Available at: https://doi.org/10.1016/s0376-7388(00)00304-5

Zhang, Yufei; Wu, Lei; Wang, Xianfeng; Yu, Jianyong; Ding, Bin (2020) 'Super hygroscopic nanofibrous membrane-based moisture pump for solar-driven indoor dehumidification', *Nature Communications*, 11(1). Available at: https://doi.org/10.1038/s41467-020-17118-3

HOW TO CITE THIS PAPER

Yang, Y., Li, S., Bouzouidja, R., Vogt-Wu, T., Lukau M'Nyampara, J., Duquesne, M. and Salagnac, P. (2026). A Photothermally Driven Moisture-Pumping Aerogel for Continuous and Directional Building Humidity Regulation. In: *Proceedings of the 22nd International Conference on Sustainable Energy Technologies (SET2026)*, Kuala Lumpur, Malaysia, 13 to 15 August 2026. Caravel Press, pp. 247–257. ISBN 978-1-995850-00-9. ISSN 2978-4387. https://doi.org/10.65582/set.2026.021

COPYRIGHT AND LICENCE

© 2026 The Author(s). This is an open access paper distributed under the terms of the Creative Commons Attribution (CC BY 4.0) licence, which permits unrestricted use, distribution and reproduction in any medium, provided the original work is properly cited.

WSSET World Society of Sustainable Energy Technologies Organised by the World Society of Sustainable Energy Technologies. Published by Caravel Press.